THE ASTROPHYSICAL JOURNAL, 559:L55–L59, 2001 September 20

SIGMOID STRUCTURE OF AN EMERGING FLUX TUBE

T. MAGARA AND D. W. LONGCOPE
Department of Physics, Montana State University, EPS 264B, P.O. Box 173840,
Bozeman, MT 59717-3840; magara@solar.physics.montana.edu
Received 2001 June 18; accepted 2001 August 3; published 2001 August 27

ABSTRACT

We present the results from three-dimensional MHD simulations of a magnetic flux tube emerging through the solar photosphere. The simulation is initialized with a straight tube of twisted magnetic field located in the upper convection zone. Buoyancy effects drive an arched segment of the tube upward through the photospheric layer and into the corona. Matter drains from the coronal field, which thereafter undergoes a rapid expansion. The coronal magnetic field formed in this manner exhibits outer poloidal field lines that resemble a potential arcade and inner toroidal field lines that emerge after the tube axis, forming sigmoid structure. The simulations suggest that the neutral-line shear and sigmoidal field arise as a natural by-product of flux emergence.

Subject headings: methods: numerical — MHD — Sun: corona — Sun: magnetic fields

1. INTRODUCTION

It is now widely believed that a magnetic field plays an important role in various activities in the solar corona. Some recent studies of coronal magnetic fields presented interesting results on the formation process of sigmoid structures observed in the corona (Matsumoto et al. 1998; Titov & Démoulin 1999; Amari et al. 2000). These sigmoid structures are suggested to have a close relation to explosive events on the Sun (Canfield, Hudson, & McKenzie 1999).

So far, the study of the dynamics of a coronal field has mainly focused on the behavior of a magnetic field above the photosphere. In such a study, a bottom boundary is located at a photospheric level in order to investigate how the magnetic field evolves above the photosphere, while the emergence of subphotospheric magnetic field into the outer atmosphere is simulated by changing the photospheric boundary condition in a particular way. The most self-consistent way to simulate the emergence of the magnetic field is to attach the convection zone below the photosphere and reproduce the emergence process directly. In order to do this, we need to know the state of the magnetic field in the convection zone. According to several studies of the dynamics of the magnetic field in the convection zone, the magnetic field rising through the convection zone has the shape of an isolated tube with a twisted magnetic field (Schüssler 1979; Choudhuri & Gilman 1987; Howard 1991; Caligari, Moreno-Insertis, & Schüssler 1995; Fisher, Fan, & Howard 1995; Longcope, Fisher, & Arendt 1996; Dorch & Nordlund 1998; Emonet & Moreno-Insertis 1998; Fan et al. 1999). Based on this result, Magara (2001) studied the evolution of a magnetic flux tube that was initially placed in the convection zone by means of 2.5-dimensional MHD simulation. Magara (2001) made a detailed investigation of the emergence and of the following expansion processes of the flux tube. This uncovered a problem in lifting the tube axis to the corona through a purely 2.5-dimensional process because the matter remaining inside a flux tube reduces the buoyancy effect on the tube. In this respect, Magara (2001) mentions several possibilities for solving this problem, one of which is to introduce a three dimensionality to the flux-tube system.

The present Letter is the first report on our work that extends Magara (2001) by including three-dimensional effects in the evolution of an emerging flux tube. We start with a straight flux tube with a uniform twist (the Gold-Hoyle flux tube) placed horizontally in the upper convection zone and follow the evolution of this tube by performing a three-dimensional MHD simulation. We find that the coronal magnetic field formed after emergence exhibits outer poloidal field lines that resemble a potential arcade and inner toroidal field lines that emerge after the tube axis, forming sigmoid structure. We show results in § 3 and discuss the formation process of sigmoid structure in § 4, after describing our simulation model in § 2.

2. SIMULATION MODEL

Our simulation code solves the three-dimensional, compressible, ideal MHD equations, including a uniform gravity. The primitive variables $\boldsymbol{v}$, $\boldsymbol{B}$, ρ, and p that are represented on a nonuniform Cartesian grid are time-advanced using the modified Lax-Wendroff method (Magara 1998). Each physical quantity is rescaled by its photospheric value. In particular, the velocity, length, and time are scaled to $C_{\rm Sp} = 8.6$ km s^{-1}, $2\Lambda_p = 300$ km, and $2\Lambda_p/C_{\rm Sp} = 35$ s (where Λ_p and $C_{\rm Sp}$ are the pressure scale height and adiabatic sound speed), respectively. The gas density and pressure are scaled to $\rho_p = 2.7 \times 10^{-7}$ g cm^{-3} and $\gamma P_p = 2 \times 10^5$ dyn cm^2. The adiabatic index takes its ideal monatomic value of $\gamma = 5/3$. The temperature and magnetic field are scaled to $T_p = 5100$ K and $(\rho_p C_{\rm Sp}^2)^{1/2} = 450$ G, respectively. The gravitational acceleration is constant throughout the domain, except near the top and bottom boundaries where gravity is zero.

We use a Cartesian coordinate system in which z increases upward, and $z = 0$ is the nominal photosphere. The domain box spans the dimensionless coordinates $(-100, -100, -10) \le (x, y, z) \le (100, 100, 100)$; it is 60×60 Mm horizontally and extends from 3 Mm below the photosphere to 30 Mm above. The grid consists of a Cartesian product in which each coordinate grid is refined toward the center. The area of finest mesh ($\Delta x = \Delta y = 0.4$, $\Delta z = 0.2$) is located within the region $(-8, -12, -10) \le (x, y, z) \le (8, 12, 10)$. The grid spacing gradually increases to $\Delta x = \Delta y = \Delta z = 4.0$ in a $N_x \times N_y \times N_z = 149 \times 167 \times 168$ grid. Periodic boundary conditions are imposed at the four sides, a fixed boundary condition at the bottom, and a free boundary condition at the top. A wave-damping zone is placed along all the boundaries to minimize their effects.

The initial condition is an isolated, twisted flux tube confined within an unmagnetized, stratified, static atmosphere. The initial atmosphere, which is identical to that used in Magara

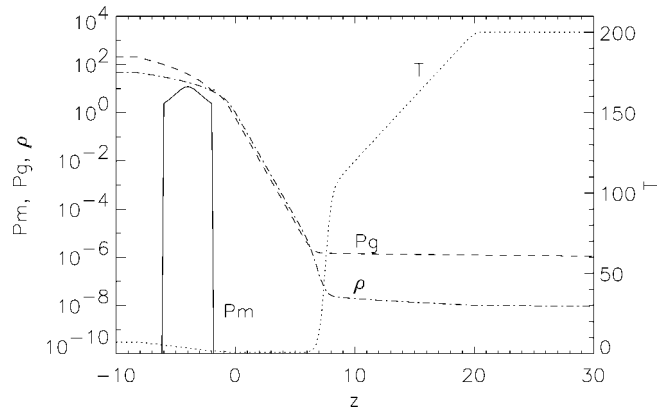

FIG. 1.—Initial distribution of physical quantities along the vertical axis. P_m, P_g, and ρ are the magnetic pressure, gas pressure, and mass density, respectively, and are plotted logarithmically against the left axis. Temperature T is plotted linearly against the right axis.

(2001), can be characterized as having a convection zone ($-10 \le z \le 0$), a photosphere at $z = 0$, a transition region around $z = 7.5$, and a corona above $z = 10$ (see Fig. 1). The initial flux tube is a uniformly twisted Gold-Hoyle equilibrium whose axis runs in the y-direction at $(x_0, z_0) = (0, -4)$ (i.e., an initial depth of 1.2 Mm) in the convection zone. The tube has a radius of $r_0 = 2$ (600 km), inside of which the gas pressure is lower than the atmosphere's in order to maintain pressure balance at the tube's surface. The magnetic field is

$$\boldsymbol{B} = \frac{B_0[-b(z - z_0)\hat{\boldsymbol{x}} + \hat{\boldsymbol{y}} + bx\hat{\boldsymbol{z}}]}{1 + b^2[x^2 + (z - z_0)^2]}, \quad \sqrt{x^2 + (z - z_0)^2} \le r_0. \quad (1)$$

Our choice of $b = 1$ implies that field lines wrap in a left-handed helix pitched over the axial length $\Delta y = 2\pi/b = 6.3$. The magnetic field on-axis, $B_0 = 17.4 = 7.8$ kG, corresponds to a local value of $\beta = 3.3$ at the center. The total axial flux of the tube, $\Phi = 3.5 \times 10^{19}$ Mx, is somewhat smaller than a full bipolar active region.

Initially, the whole system is in mechanical equilibrium. The atmosphere outside the tube is in hydrostatic balance, and the magnetic field within the tube is force-free. The total pressure is continuous across the tube's surface because of a discontinuity in gas pressure there: the temperature inside the tube is lower than outside the tube. Since the Gold-Hoyle magnetic field is weakly unstable to current-driven kink instabilities (Linton, Longcope, & Fisher 1996), the dominant source of instability is the Parker instability (Parker 1966). The purpose of the present study is not, however, to study the instability of the tube but rather to observe its emergence into the corona. Toward this end, we initiate the Parker instability by firmly driving the middle portion of the tube upward and the ends downward for an interval $0 \le t \le t_0$. The fluid velocity,

$$v_z(x, y, z, t) = \begin{cases} \dfrac{\pi}{2t_0} \cos\left(2\pi \dfrac{y}{\lambda}\right) \sin\left(\dfrac{\pi}{2} \dfrac{t}{t_0}\right), & -\dfrac{\lambda}{2} \le y \le \dfrac{\lambda}{2}; \\ -\dfrac{\pi}{2t_0} \sin\left(\dfrac{\pi}{2} \dfrac{t}{t_0}\right), & \text{otherwise,} \end{cases} \quad (2)$$

is prescribed ($t_0 = 5$ and $\lambda = 30$) within the fixed volume $x^2 + (z - z_0)^2 \le r_0^2$, and the usual momentum equation is used outside. We observe a steep gradient in velocity at the edge of

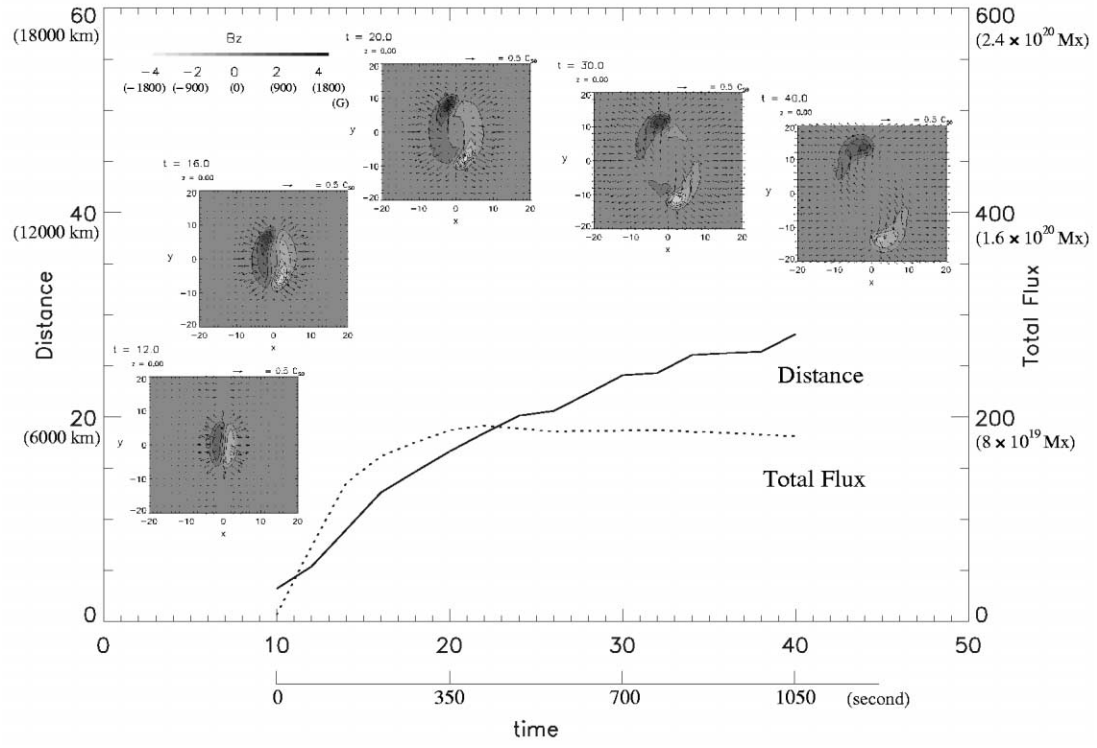

FIG. 2.—Time sequence of flux emergence characterized by using the magnetic field at the photospheric plane ($z = 0$). The total unsigned flux vs. distance (*dotted line, right axis*) shows the flux crossing the plane at $t = 10$ and the axis crossing the plane by $t \simeq 20$. A second horizontal axis gives the time in seconds beginning at the moment of emergence. The separation distance (*solid line, left axis*) is found from a B_z-weighted position average in the immediate neighborhood of the extreme pixel. The insets show B_z (*contours and gray scale*), and $v_\perp$ (*arrows*) are the times $t = 12$, 16, 20, 28, and 40.

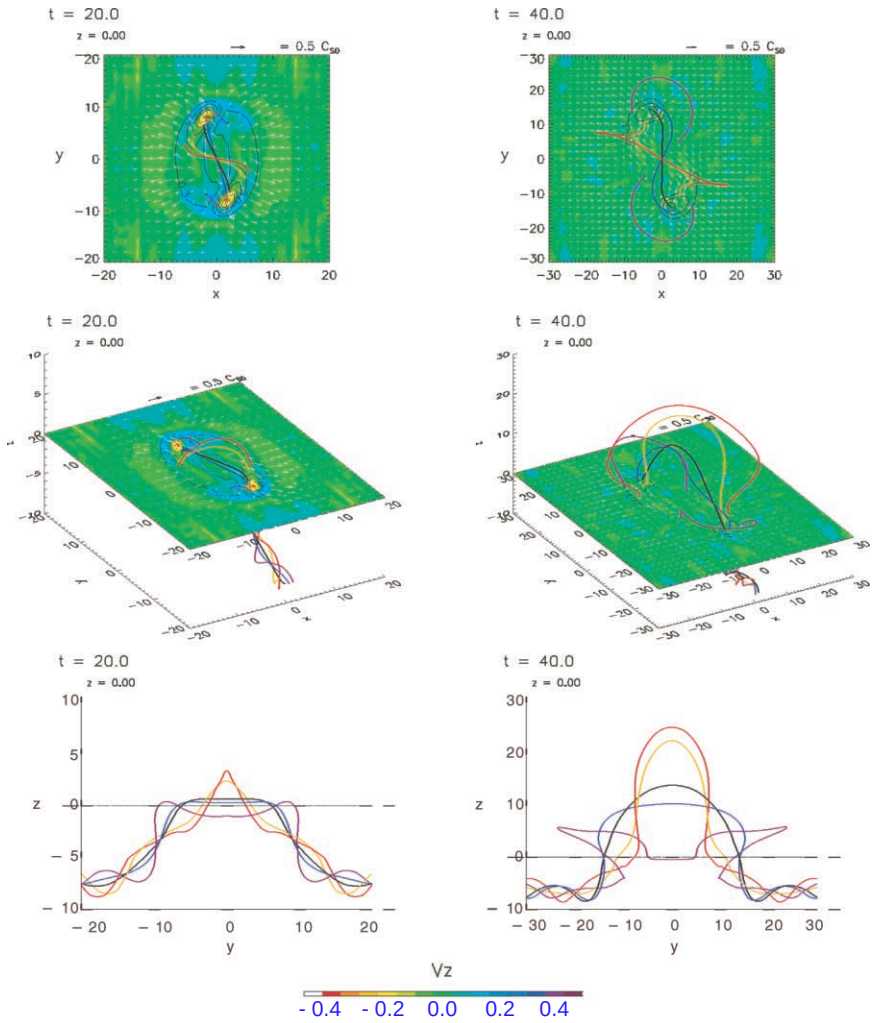

FIG. 3.—*Top left panel*: Top-view snapshot of the magnetic field lines (*colored lines*), horizontal velocity field (*white arrows*), vertical velocity (*color map*), and vertical magnetic field (*contour lines*; contour interval is 0.6) taken at $t = 20$. The two-dimensional plane is located at $z = 0$. *Top right panel*: Top-view snapshot taken at $t = 40$. *Middle left panel*: Perspective-view snapshot taken at $t = 20$. *Middle right panel*: Perspective-view snapshot taken at $t = 40$. *Bottom left panel*: Side-view snapshot taken at $t = 20$. *Bottom right panel*: Side-view snapshot taken at $t = 40$. Each colored field line is drawn by a Lagrangian tracing method, and the black line shows the tube axis.

the driven region during the period of driving. After the driving period, $t > t_0$, the region is advanced according to the momentum equation, and we find that the steep gradient has almost disappeared by $t = 10$, in a couple of sound relaxation times.

3. RESULTS

After the initial driving phase, the flux tube continues upward and emerges into the unmagnetized corona. The flux emergence is depicted in Figure 2 using the horizontal velocity and vertical magnetic field at the photospheric plane $z = 0$. Once the edge of the tube crosses the photosphere, at $t \simeq 10$, the total unsigned flux grows steadily, reaching its maximum value 350 s (10 time units) later, after the tube's axis crosses the photosphere. The vertical magnetic field forms a classic magnetic bipole. The bipole is initially oriented perpendicular to the tube's axis because of the strongly azimuthal nature of the field at its edge. During emergence, the opposing polarity regions separate and rotate toward a more axial ($\hat{y}$) orientation (Fan 2001). The separation, specifically the distance between points of maximum positive and negative B_z, increases throughout the simulation but slows toward the end.

Figure 3 shows coronal magnetic field lines at two times during the tube's emergence. The first snapshot ($t = 20$, *left panels*) is just after the emergence of the tube's axis; the second snapshot ($t = 40$, *right panels*) is well past the axis emergence. Selected field lines, traced in colored lines, are shown from a top view (*upper panels*), a perspective view (*middle panels*) and a side view (*bottom panels*). At $t = 40$, most but not all of the magnetic field lines cross into the corona. The vertical and horizontal components of velocity at the $z = 0$ plane are shown with colors and white arrows, respectively. A strong draining downflow ($v_z \simeq -2$ km s^{-1}) is evident near the footpoints, $(x, y) = (\pm 2, \mp 8)$, in the early snapshot but has largely subsided by the later one.

In the early snapshot, the outermost field is almost perpendicular to the neutral line (y-axis), while the inner field is more parallel to the neutral line. This probably reflects the fact that the inner field lines, closer to the tube's axis, are more axial, while the outer field lines are more azimuthal. After the axis emerges (*right panels*), the inner field lines show a distinct inverse S shape reminiscent of sigmoid structures observed by the soft X-ray telescope on board *Yohkoh* (Fig. 4*a*). In contrast to the inner field lines, the outer field lines form a potential-like arcade with a forward S shape. These contrasting field-

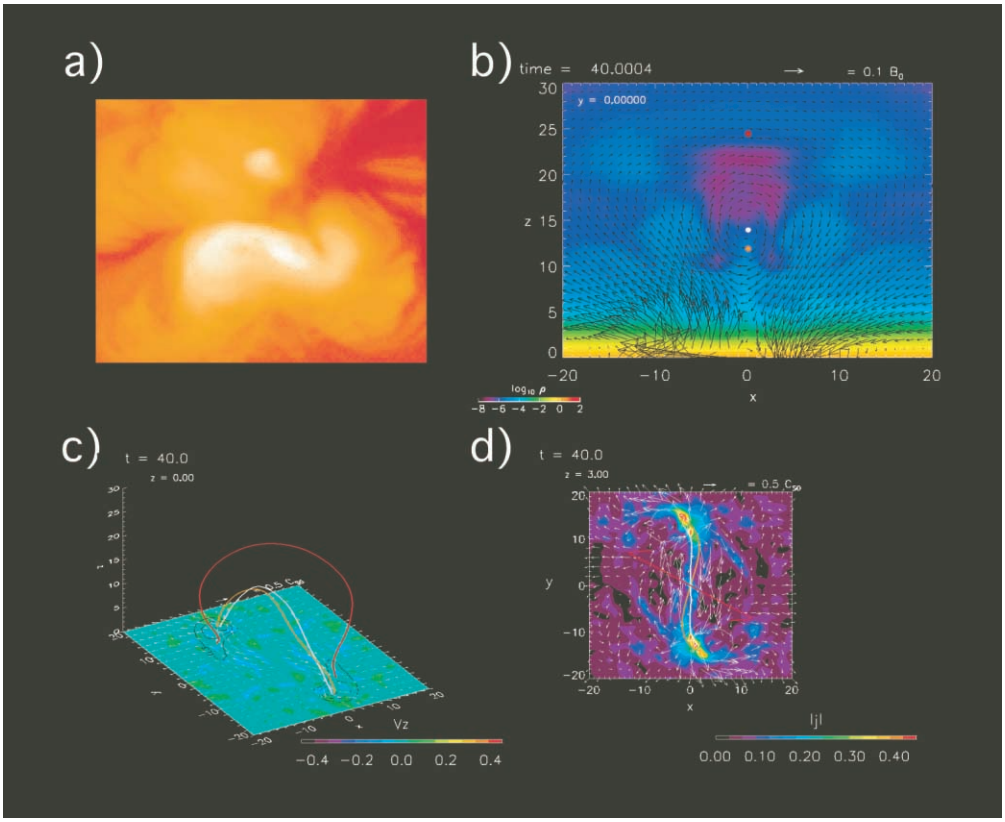

FIG. 4.—(*a*) Example of a sigmoid structure taken by the soft X-ray telescope on board *Yohkoh*, courtesy of the *Yohkoh* team members. (*b*) Two-dimensional view of the magnetic field projected onto the $y = 0$ plane (*black arrows*) and the density (*color map*) at $t = 40$. (*c*) Perspective-view snapshot of the three magnetic field lines (*red, white, and orange lines*), horizontal velocity field (*white arrows*), vertical velocity (*color map*), and vertical magnetic field (*contour lines*; contour interval is 0.6) taken at $t = 40$. The two-dimensional plane is located at $z = 0$. The position where each field line penetrates the $y = 0$ plane is marked in (*b*) with a dot of the same color as the field line. (*d*) Top-view version of (*c*), but a color map shows the absolute value of the current density measured at $z = 3$.

line configurations can be attributed to the fact that a potential-like arcade structure is formed by the outermost azimuthal field lines of the flux tube while a sigmoid structure is made of the axial field lines near the tube's axis.

The contrasting field lines in the postemergence field are shown more clearly in Figures 4*b*–4*d*. Figure 4*b* shows the magnetic field (*black arrows*) and mass density (*color scale*) within the $y = 0$ vertical midplane at $t = 40$. The twisted flux-tube structure is clearly visible as arrows circulating clockwise about a central point at $z = 14$, about 4.2 Mm above the photosphere. Above the central point, the density has been greatly depleted by expansion and draining. Three magnetic field lines were selected according to their location within the midplane (Fig. 4*c*). The white field line is the tube's center, where the magnetic field is normal to the plane. The red and orange field lines cross the midplane directly above ($z = 24.5$) and below ($z = 12$) the center point. A top view of each field line (Fig. 4*d*) shows that the lower lying orange field line forms an inverse S while the higher red field line forms a tightly curved forward S. Both field lines wrap leftward around the much straighter central field line (*white*).

4. DISCUSSION

Observational studies have shown that active regions with negative helicity ($\alpha < 0$) have soft X-ray loops with inverse S shapes (Canfield et al. 1999). Our simulation begins with a flux tube twisted in the left-handed sense, and its emergence produces photospheric fields characterized by negative "observed" values of α. Notably, the coronal field contains both forward and inverse S shapes. To reconcile these simulations with observation, it is necessary to explain why the inverse S field would be most visible in soft X-ray images.

Several recent studies have shown the formation of sigmoids in the magnetic field. Matsumoto et al. (1998) show by simulation that a sigmoid is produced by a twisted flux tube that emerges after undergoing the kink instability. Amari et al. (2000) construct a force-free coronal field with sigmoid structure and discuss the stability of this solution. In each of these studies, only the shape of field line is discussed, so the soft X-ray emission is not an issue. Titov & Démoulin (1999) investigate the three-dimensional shape of the separatrix surface formed inside a magnetic structure. They show that the separatrix has an inverse S shape and appeal to the notion that reconnection would occur in its vicinity. This explains both the formation and the illumination of the sigmoid.

If the process of energization is considered, the active region formed in our simulation would appear as an inverse S in soft X-ray images. Those field lines exhibiting an inverse S configuration are also the field lines on which energy deposition would occur. Figure 4*d* shows a top view of the three field lines over a color map of current density $|\boldsymbol{J}|$ at the lower chromosphere ($z = 3$, i.e., 900 km above the photosphere). From this color map, it is evident that high current densities are concentrated at the footpoint of an inverse S-shaped field line (*orange line*). Although the precise mechanism by which coronal loops brighten remains uncertain, one study finds a

direct link between coronal heating and the current measured at the lower atmosphere (Lee et al. 1998). Accepting this result, we can assume then that the strong concentration of current density at the footpoint of inverse S-shaped field lines could provide a significant heat source for these lines. Furthermore, this result also presents an idea for solving the problem of why only inverse S-shaped field lines are strongly brightened so as to be observed as a sigmoid.

In summary, we have simulated the emergence of a twisted flux tube into the corona using a three-dimensional, time-dependent code. After emergence, the outer azimuthal field of the tube expands to form a potential-like arcade structure naturally, while the inner axial field that emerges after the tube axis produces a twisted sigmoidal structure. The low-lying inner field lines originate from regions of the highest current concentration and therefore will be the most visible in coronal emission such as soft X-rays.

This work was supported by AFOSR grant F49620-00-1-0128. The numerical computations have been carried out by using NEC SX-5 at the National Institute of Fusion Science in Japan and Cray J924se at the National Center for Atmospheric Research in the US.

REFERENCES

Amari, T., Luciani, J. F., Mikic, Z., & Linker, J. 2000, ApJ, 529, L49
Caligari, P., Moreno-Insertis, F., & Schüssler, M. 1995, ApJ, 441, 886
Canfield, R. C., Hudson, H. S., & McKenzie, D. E. 1999, Geophys. Res. Lett., 26, 627
Choudhuri, A. R., & Gilman, P. A. 1987, ApJ, 316, 788
Dorch, S. B. F., & Nordlund, Å. 1998, A&A, 338, 329
Emonet, T., & Moreno-Insertis, F. 1998, ApJ, 492, 804
Fan, Y. 2001, ApJ, 554, L111
Fan, Y., Zweibel, E. G., Linton, M. G., & Fisher, G. H. 1999, ApJ, 521, 460
Fisher, G. H., Fan, Y., & Howard, R. F. 1995, ApJ, 438, 463
Howard, R. F. 1991, Sol. Phys., 136, 251
Lee, J., McClymont, A. N., Mikic, Z., White, S. M., & Kundu, M. R. 1998, ApJ, 501, 853
Linton, M. G., Longcope, D. W., & Fisher, G. H. 1996, ApJ, 469, 954
Longcope, D. W., Fisher, G. H., & Arendt, S. 1996, ApJ, 464, 999
Magara, T. 1998, Ph.D. thesis, Univ. Kyoto
Magara, T. 2001, ApJ, 549, 608
Matsumoto, R., Tajima, T., Chou, W., Okubo, A., & Shibata, K. 1998, ApJ, 493, L43
Parker, E. N. 1966, ApJ, 145, 811
Schüssler, M. 1979, A&A, 71, 79
Titov, V. S., & Démoulin, P. 1999, A&A, 351, 707